Ultrasonics Sonochemistry 98 (2023) 106499

Contents lists available at ScienceDirect

Ultrasonics Sonochemistry

journal homepage: www.elsevier.com/locate/ultson

Continuous sonochemical nanotransformation of lignin – Process design and control

Sílvia Pérez-Rafael [a], Guillem Ferreres [a], Rudolf W. Kessler [b], Waltraud Kessler [b], Jeniffer Blair [a], Garima Rathee [a], Angela Gala Morena [a], Tzanko Tzanov [a,*]

[a] Grup de Biotecnologia Molecular i Industrial, Department of Chemical Engineering, Universitat Politècnica de Catalunya, Rambla Sant Nebridi 22, Terrassa 08222, Spain

[b] Kessler ProData GmbH, Kaiserstr. 66, Reutlingen 72764, Germany

ARTICLE INFO

Keywords:
Lignin
Nanoparticles
Ultrasound
DoE
UV–Vis spectroscopy
Modelling

ABSTRACT

As the most abundant renewable aromatic polymer on the planet, lignin is gaining growing interest in replacing petroleum-based chemicals and products. However, only <5 % of industrial lignin waste is revalorized in its macromolecular form as additives, stabilizing agents or dispersant and surfactants. Herein, revalorization of this biomass was achieved by implementing an environmentally-friendly continuous sonochemical nanotransformation to obtain highly concentrated lignin nanoparticles (LigNPs) dispersions for added-value material applications. With the aim to further model and control a large-scale ultrasound-assisted lignin nanotransformation, a two-level factorial design of experiment (DoE) was implemented varying the ultrasound (US) amplitude, flow rate, and lignin concentration. Size and polydispersity measurements together with the UV–Vis spectra of lignin recorded at different time intervals of sonication allowed to monitor and understand the sonochemical process on a molecular level. The light scattering profile of sonicated lignin dispersions showed a significant particle size reduction in the first 20 min, followed by moderate particle size decrease below 700 nm until the end of the 2 h process. The response surface analysis (RSA) of the particle size data revealed that the lignin concentration and sonication time were the most important factors to achieve smaller NPs. From a mechanistic point of view, a strong impact of the particle–particle collisions due to sonication seems to be responsible for the decrease in particle size and homogenization of the particle distribution. Unexpectedly, a strong interaction between the flow rate and US amplitude on the particle size and nanotransformation efficiency was observed, yielding smaller LigNPs at high amplitude and low flow rate or *vice versa*. The data derived from the DoE were used to model and predict the size and polydispersity of the sonicated lignin. Furthermore, the use of the NPs spectral process trajectories calculated from the UV–Vis spectra showed similar RSA model as the dynamic light scattering (DLS) data and will potentially allow the in-line monitoring of the nanotransformation process.

1. Introduction

Lignin is an aromatic biopolymer representing 15–30 % of the dry mass of plants [1,2]. The paper manufacturing industry generates nearly 70 million tons of lignin each year [3] as a low-value by-product usually used for energy recovery or transformed through biorefinery approaches into small molecular weight phenolics [4]. Only 2–5 % of lignin waste is revalorized in its macromolecular form [5]. Rising environmental concerns and depletion of petro-chemical resources have boosted the interest of using bio-renewable polymers to prepare high-performance composite bio-based materials. Considerable efforts have been made to propose potential uses of lignin waste as fillers for preparation of polyurethane foams, fiber mats, and thermoplastics materials, due to its high abundance, low weight, carbon neutrality, biodegradability and

Abbreviations: DLS, dynamic light scattering; DoE, design of experiment; HD, hydrodynamic diameter; LigNPs, lignin nanoparticles; LigPs, large lignin particles; LigSol, soluble lignin; MCR, multivariate curve resolution; ML, machine learning; NPs, nanoparticles; PAT, process analytical technology; PDI, polydispersity index; RSA, response surface analysis; US, ultrasound; UV, ultraviolet; UV-Vis, ultraviolet-visible.

* Corresponding author.
E-mail address: tzanko.tzanov@upc.edu (T. Tzanov).

https://doi.org/10.1016/j.ultsonch.2023.106499
Received 31 March 2023; Received in revised form 5 June 2023; Accepted 19 June 2023
Available online 21 June 2023

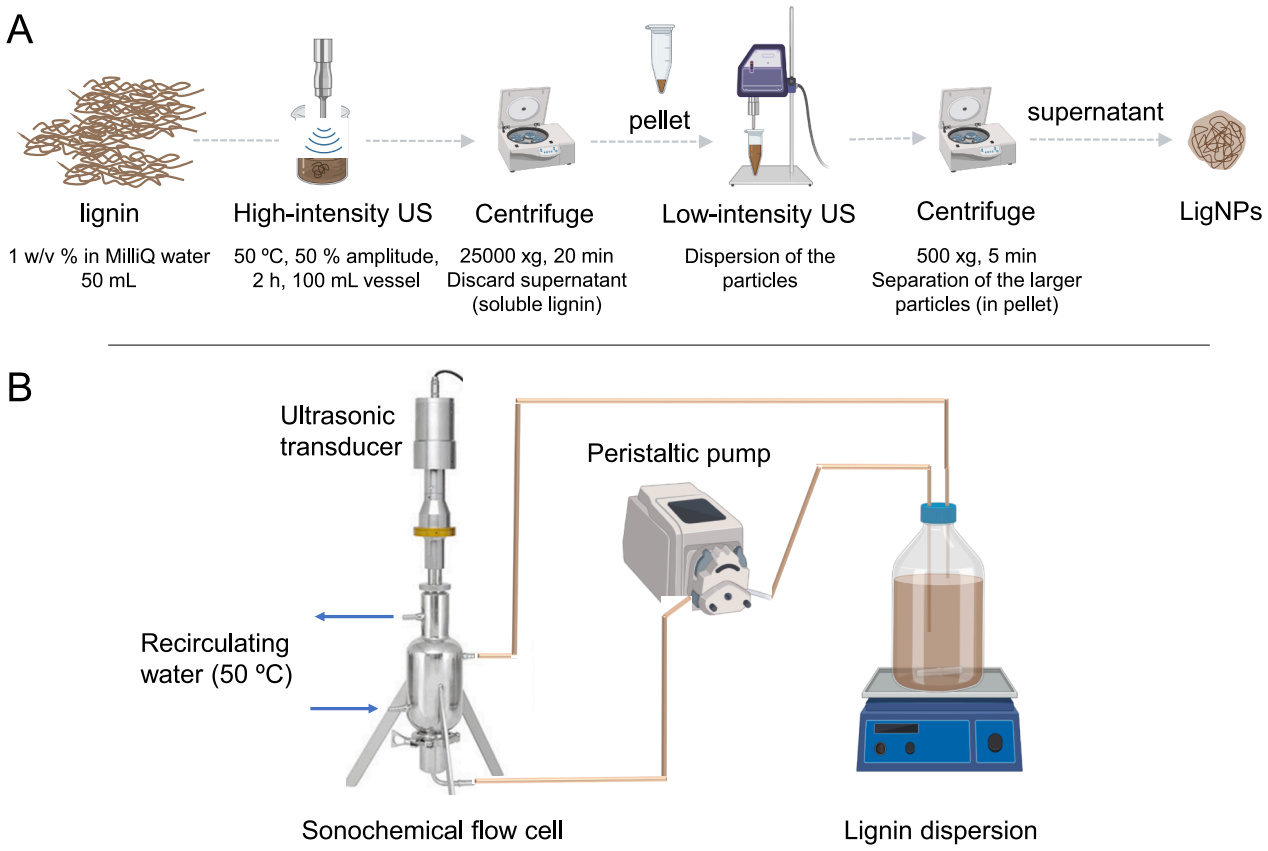

Fig. 1. A) Overall procedure for obtaining LigNPs in a lab-scale batch process. B) Schematic representation of the sonochemical reactor set-up in continuous flow and samples characterization.

reinforcing capability [6–8]. However, its low compatibility with polymeric matrices in composite production and its heterogeneous molecular structure, which heavily depends on the extraction and purification processes, are the key reasons for its underutilization and limited applications.

Besides the structural role of lignin in plants, it also provides defense against bacterial and fungal pathogens, [9,10] antioxidant [11] and UV-blocking capacities [12,13] conferred by the phenolic hydroxyl groups in its structure. On the other hand, these phenolic functionalities also allow for further modification of lignin enabling different applications as an active ingredient, especially in the form of nanoparticles (NPs) [14]. Nanotransformation is an emerging valorization approach that produces lignin NPs (LigNPs) with higher interfacial reactivity compared to their bulk counterparts. Addition of LigNPs in composite materials endows them with improved mechanical properties and bioactivities [15]. For instance, LigNPs have been used as structural fillers in polymer matrices [16], antibacterial and antioxidant actives in food packaging [17] or biomedical applications [18,19], UV absorbents [20,21], and as carriers for drug delivery [22].

Solvent displacement [23], acid precipitation [24], sonochemistry and combinations thereof are the most common techniques for synthesizing LigNPs. The environmentally safe waterborne sonochemical process can simultaneously synthesize and coat nanoparticles on surfaces without the need for any additives. It has been selected by IUPAC among the top ten emerging technologies in chemistry for 2021 [25]. During ultrasonication, NPs are obtained by fractioning the large lignin macromolecule due to the cavitation phenomena [26,27] achieving higher yield in comparison to the other methods – a prerequisite for potential industrial application.

The possibility to sonochemically produce highly reactive lignin NPs opens the way for a wide use of this bio-based waste material in many new applications. However, for an industrial use of sonochemical processes, ways have to be found to achieve high throughput of NPs production for cost reduction, while maintaining consistent quality for manufacturing high-added-value products, e.g., lightweight composites for the automotive sector [28]. Therefore, this work aims to acquire a deeper understanding of the sonochemical process for lignin nanotransformation based on its monitoring and control on a molecular level. To this end, methods of statistical design of experiments (DoE) allowing to assign both qualitatively and quantitatively "cause and effect" will be used. Optical spectroscopy together with complex multivariate data analysis will provide efficient inline quality control to generate knowledge from data on a molecular level and to visualize *in-situ* chemical and morphological changes in lignin during the nanotransformation process [29].

2. Materials and methods

2.1. Materials

Protobind^{TM} 6000 soda lignin was purchased from PLT innovations (Switzerland). Protobind^{TM} 6000 is a sulphur-free product obtained from agricultural fibrous feedstocks, with Mn ~1000 g/mol, Mw ~3500 g/mol, aliphatic OH content 2.6 mmol/g, phenolic OH content ~2.9 mmol/g, and acid OH content ~0.8 mmol/g.

2.2. Synthesis of LigNPs

2.2.1. Sonochemical batch process

In a preliminary lab-scale batch process, 50 mL dispersion of commercially available soda lignin at 10 g/L was subjected to high-intensity ultrasound (20 kHz, Ti-horn) at 50 % amplitude and 50 °C

Table 1
Summary of the DoE variables for continuous sonochemical production of LigNPs.

Factor	Units	Minimum	Maximum	Mean
A: Amplitude	%	20	50	35
B: Flow rate	rpm	50	150	100
C: Lignin concentration	g/L	10	30	20

Table 2
Experiments according to the DoE for continuous sonochemical production of LigNPs.

	Factor 1	Factor 2	Factor 3
Run	**A: Amplitude (%)**	**B: Flow rate (rpm)**	**C: Lignin concentration (g/L)**
1	35	100	20
2	20	50	30
3	50	150	10
4	20	150	10
5	50	50	30
6	35	100	20
7	50	50	10
8	20	50	10
9	20	150	30
10	50	150	30
11	35	100	20

for 2 h to synthesize LigNPs (Fig. 1A), following an adapted previously reported protocol [26]. The mixture was centrifuged at 25,000 *g* for 20 min to remove the supernatant corresponding with the soluble lignin fraction (LigSol). The pellet was resuspended in water and then, disaggregation of the particles was achieved by applying low-intensity ultrasound. At last, the NPs were centrifuged at 500 *g* for 10 min to remove larger aggregates.

2.2.2. Sonochemical continuous process

In order to produce LigNPs at larger scale, 2 L of lignin dispersions of different concentrations (10 – 30 g/L) (Table 2) were recirculated using a peristaltic pump GP1100 (Fisher Scientific, Spain) through a 500 mL cylindrical sonochemical flow cell (Sonics & Materials, inc, USA) equipped with a jacket for temperature control and containing a 25 mm high efficiency ultrasonic probe. This cell operates in a continuous-mode and is equipped with a 1500-Watt piezoelectric ultrasonic transducer with a frequency of 20 kHz (Sonics & Materials, inc, USA). Temperature control in the cell was provided by recirculation of water at 50 °C using an Accel 500 LC chiller (Thermo Scientific, Spain). Additionally, the ultrasound probe was cooled by pressurized air (0.4 bar) (Fig. 1B).

A key parameter of the continuous sonication process is the flow rate of recirculating the lignin dispersion and consequently the residence time and the number of cycles it stays in the reactor. The measured flow rates were: 222, 364, and 728 mL/min at 50, 100, and 150 rpm, respectively.

After sonication, three different fractions corresponding to the soluble lignin (LigSol), larger lignin particles (LigPs) and LigNPs were

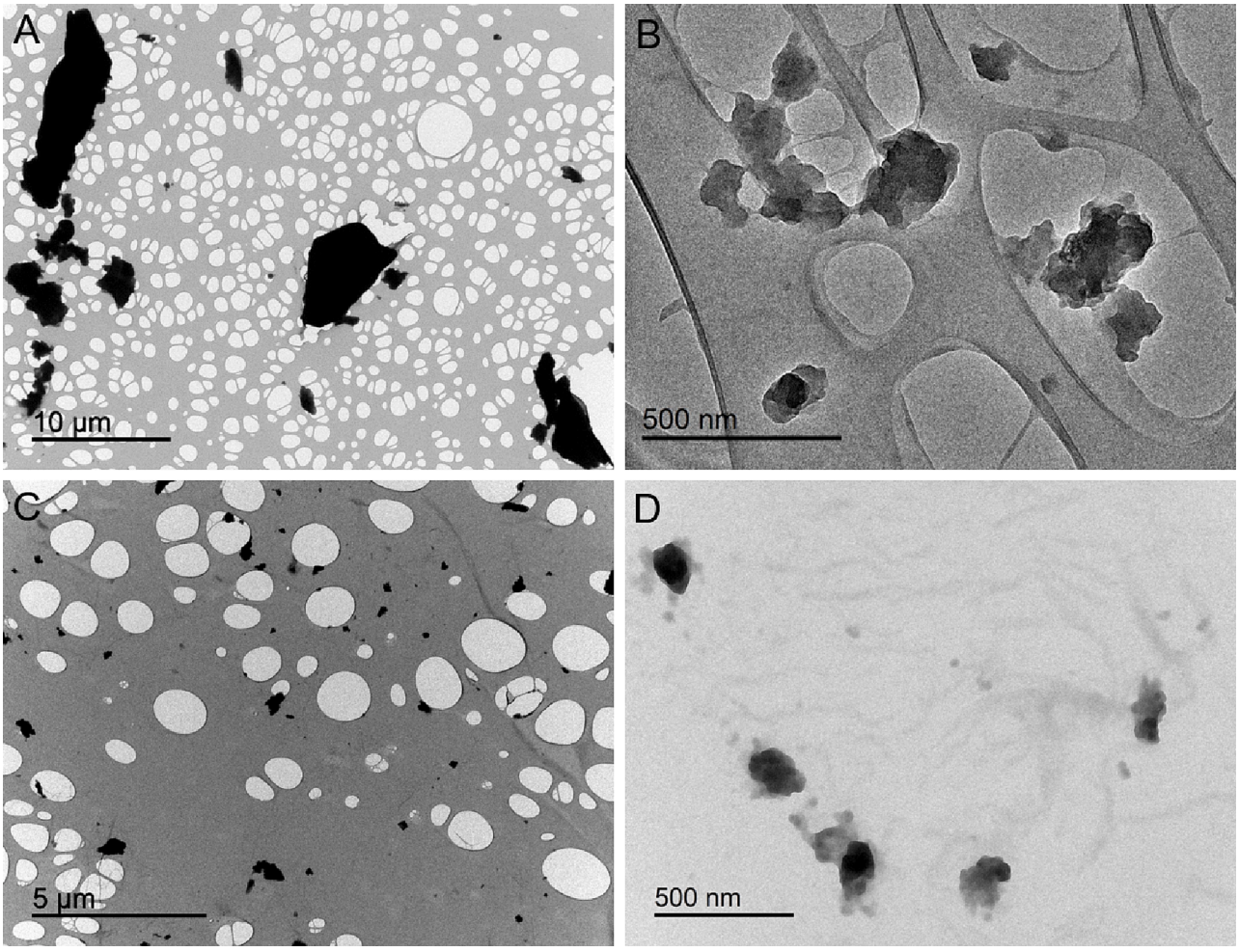

Fig. 2. TEM images of A) lignin in bulk form, B) LigNPs obtained in a batch process, and C), D) showing lignin particles and NPs obtained after 2 h of lignin sonication in continuous mode.

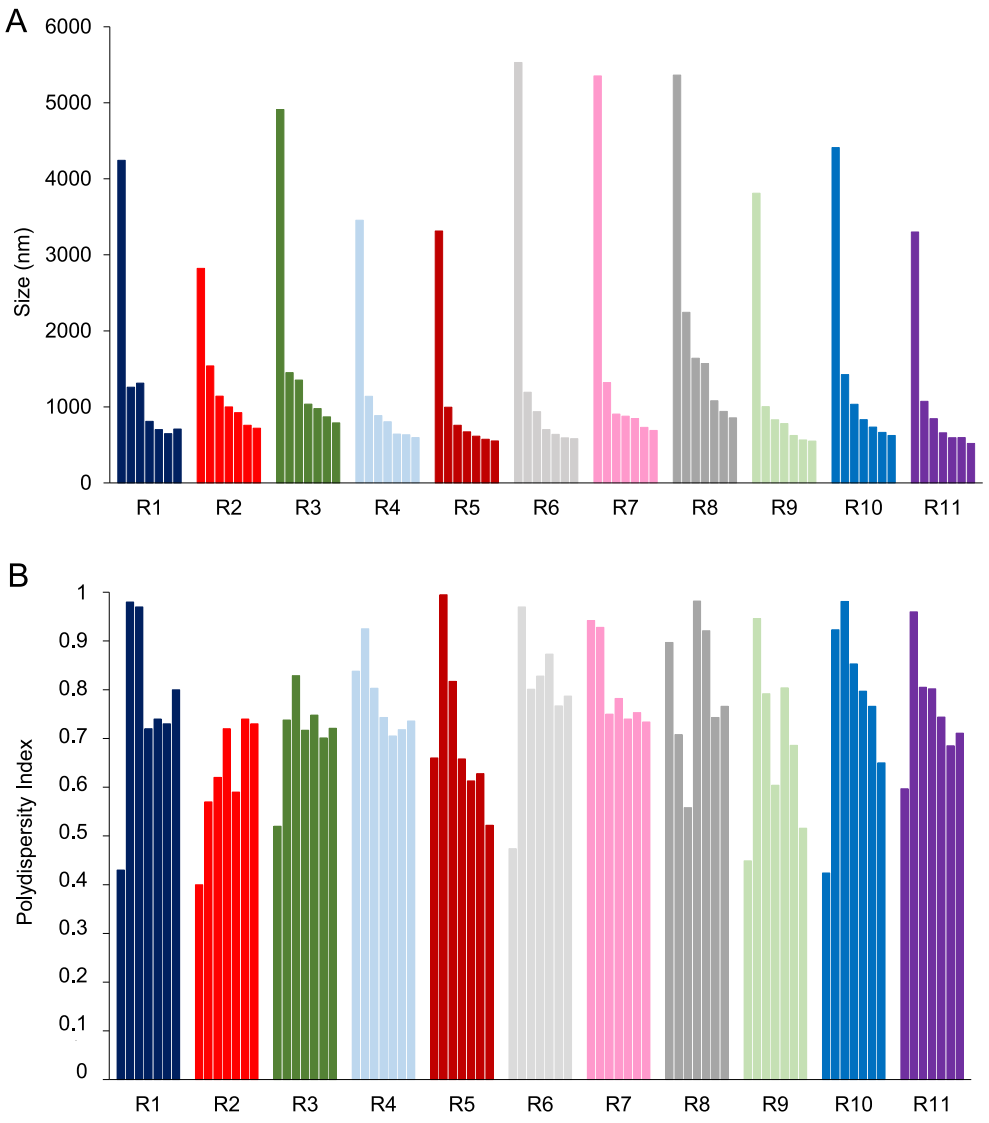

Fig. 3. A) Average particle size (nm) and B) Polydispersity index (PDI) for all 11 runs measured every 20 min by DLS in the whole fraction of sonicated lignin. Time interval measured: t = 0 to t = 120 min.

Table 3
Coefficients of regression model terms of the response surface analysis for response ln(DLS size).

Intercept: +6.81	A-US Amplitude: −0.033
B-Flow rate:-0.057	C-Lignin concentration: −0.10
D- Reaction time: −0.42	AB-interaction:+0.16

obtained by two sequential centrifugation steps. First, 15 mL of lignin suspensions were centrifuged at 25,000 *g* for 40 min to obtain the supernatant corresponding with the soluble lignin fraction. Afterwards, the pellet was resuspended in 15 mL of MilliQ water and the particles disaggregated by applying low-intensity ultrasound for 30 s. Then, the resulting mixture was subjected to a moderate centrifugation (500 *g* for 5 min) to separate the larger aggregates from the LigNPs. Finally, all the samples were freeze-dried and weighed to estimate the wt% of each fraction.

2.3. Design of experiments (DoE) and sampling

Based on lab-scale experiments, three parameters were selected and tested for optimization of the LigNPs synthesis: ultrasonic (US) amplitude (%), flow rate (rpm), and lignin concentration (g/L). A two-level factorial design with 3 center points was set up, which resulted in 11 randomly executed runs (Tables 1 and 2). The lignin dispersions were subjected to sonication for 2 h upon recirculation. Samples were collected every 20 min and immediately analyzed by dynamic light scattering (DLS) and UV–Vis spectroscopy. Thus, a fourth factor reaction time is added to the existing three factor design. This factor is varied on 7 different levels, which represent reaction time (samples at reaction time every 20 min starting from t = 0 until t = 120 min reaction time.) For UV–Vis analysis, a 2 μL sample was diluted in 2 mL MilliQ water, while for DLS measurements, a 100 μL sample was diluted in 1.5 mL MilliQ water.

The set up of the design and the analysis of the responses is done with the software package Design Expert Version 10 (Stat Ease Inc., Minneapolis, MN, USA).

2.4. Dynamic light scattering (DLS) particle characterization

The particle size distribution analysis of the sonicated lignin dispersions was performed by DLS (Zetasizer, Malvern, Germany). The sample was 20-fold diluted with MilliQ water in polystyrene cuvettes (Sardest, Spain). The measurements were performed at 25 °C and the

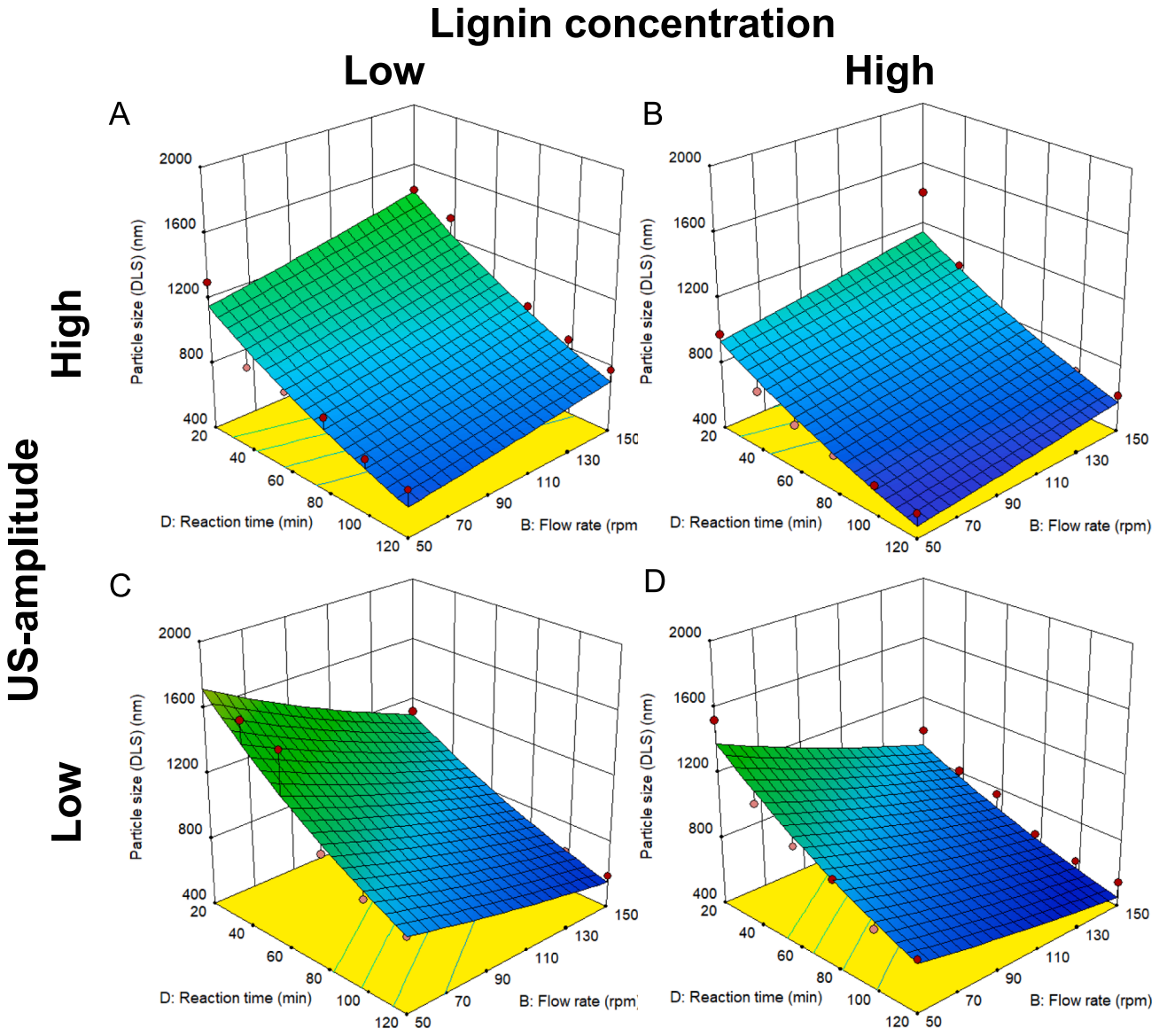

Fig. 4. Response surface-plots of particle size model: A) and B) with high US-amplitude, C) and D) with low US-amplitude; A) and C) with low lignin concentration and B) and D) with high lignin concentration. DLS data for t = 20 to t = 120 min.

data were analyzed by setting the refraction index of the sample to 1.6.

2.5. UV–Vis spectroscopy

The lignin samples were diluted 1000-fold and subsequently analyzed at-line spectrophotometrically in transmission mode (10 mm quartz cuvette, Helma Germany,) with a Varian Cary 100 Bio spectrophotometer (Varian, Australia) in the wavelength range 200–800 nm. Water was used as a reference and the spectral resolution was set to 2 nm.

2.6. Multivariate curve resolution (MCR)

MCR of the UV–Vis spectra was performed using the Unscrambler® X 10.5 software package (CAMO Software AS, Norway). The spectra in the region 200–800 nm were normalized (unit vector normalization) before chemometric analysis to compensate for intensity shifts caused by dilution of the dispersions and possible sedimentation during the measurements. Preliminary studies using principal component analysis of the spectral features suggested to use a 3-component extraction as a start: soluble lignin, lignin particle distribution with a bias towards larger particle size, and lignin particle distribution with a bias towards smaller particle size within the nanoparticle range. For the MCR analysis, non-negativity and closure were applied as constraints.

2.7. Morphological characterization of the NPs

A JEOL JEM-1010 transmission electron microscope (TEM) was used to assess the size and morphology of the lignin NPs. The images were acquire by a CCD Orius camera (Gatan). The samples were placed on a holey carbon grid and the microscope was operated at an accelerating voltage of 80 kV.

3. Results and discussion

3.1. Morphological characterization and quantification of the lignin fractions

3.1.1. Morphological characterization of the lignin particles

The lab-scale batch process production of LigNPs demonstrated that

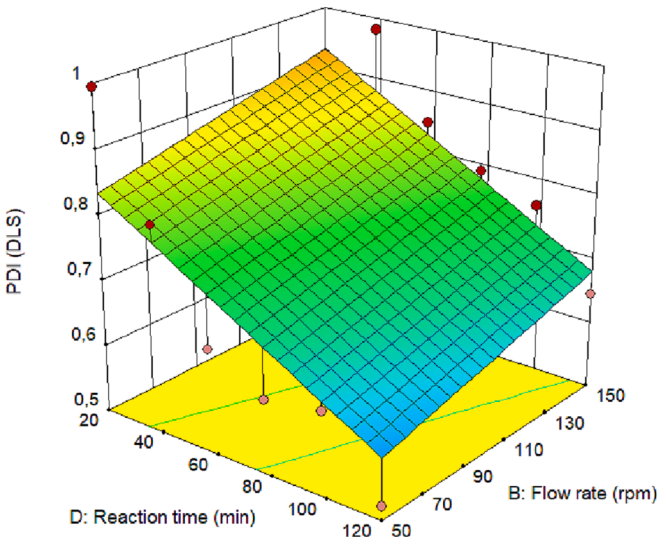

Fig. 5. Response surface analysis using PDI data for t = 20 to t = 120 min of runs no. 1 – 11 with high setting of lignin concentration, and high US amplitude.

the energy generated during the cavitation process was sufficient to fragment the bigger particles of the lignin biomass yielding NPs in a waterborne environmentally friendly procedure (Fig. 2A and B). As described in previous reports [26,27,30], TEM images showed how cavitation phenomena caused by the application of US waves disintegrated lignin macromolecules generating non-regular shape NPs with an average size around 200 nm. Similarly, TEM images corresponding to lignin dispersions obtained after 2 h of continuous sonication presented lignin particles with sizes ranging from approximately 850 to 150 nm (Fig. 2C and D).

The determination of the absolute particle size and particle size distribution by dynamic light scattering (DLS) or optical spectroscopy is for orientation only when analyzing amorphous and unstructured systems, such as the lignin particles. The prerequisites applied to the models, e.g., a homogeneous and spherical particle structure, are not always fulfilled. Nevertheless, DLS and optical spectroscopy could be of great use for at-line or in-line quality control to detect and follow trends in the evolution of product quality during processing. Often it will be sufficient to establish a so-called "golden batch" which defines the limits (e.g., process trajectories) in which the process should perform [29]. Thus, the objective of these experiments was to get insight into the structure and absolute particle size of the original lignin material and the lignin subjected to sonication. The great advantage using in-line spectroscopy is the possibility to establish a 100 % quality control, whereas at-line techniques such as TEM may lack representativeness due to an insufficient number of samples.

3.1.2. Quantification of the fractions of soluble lignin, larger lignin and lignin NPs

The percentage of soluble, larger and smaller lignin particles can be estimated after sequential centrifugation steps. The procedure is highly time consuming and thus, only 5 out of the 11 runs were analyzed in this way defining 25 – 35 % soluble lignin, 5–15 % lignin NPs in the supernatant and 55–70 % larger lignin fragments. A more detailed discussion will be presented in the spectroscopic section where data from all runs are collected together with their evolution during processing.

3.2. DLS at-line monitoring during sonication and response surface analysis (RSA)

3.2.1. Particle size and polydispersity

DLS is a powerful tool for the determination of NP size, size distribution and colloidal stability during nanomaterial preparation. The method provides simultaneously the average particle hydrodynamic diameter (HD) and polydispersity index (PDI) - crucial parameters for the chemical and physical properties of nanomaterials. The PDI is a measure of the heterogeneity of a sample based on size. Polydispersity can occur due to particle agglomeration during isolation, purification or analysis. An industrial sonochemical process for lignin nanotransformation requires the consistent production of small LigNPs in a short time at the highest possible concentration of the starting material to ultimately achieve high throughput, thus saving production costs.

From the sample every 20 min aliquots were withdrawn. In the aliquots larger and smaller LigNPs together with bulk lignin were simultaneously present. The light scattering profile of lignin dispersions before and after ultrasonication (Fig. 3A) showed a significant particle size reduction from more than 2500 nm to about 1000 nm during the first 20 min in most cases. Beyond 20 min sonochemical treatment, the particle diameters decreased exponentially following a first-order kinetics until the end of the 2 h process, reaching sizes below 700 nm [31]. These findings suggest the option for considerably shortening of the sonochemical nanotransformation process. A good compromise between a lower size (e.g., 700 nm) and an acceptable PDI (e.g., below 0.7) may be achieved within 60 min by optimum parameter settings (see optimization) that increase the throughput of the sonication process.

However, the still rather high PDI (Fig. 3B) indicates also a broad particles size distribution in the samples. Thus, modelling of the nanotransformation process using size data instead of PDI data, should be preferred for the sake of model robustness. Despite that the irregular morphology of the lignin particles observed by TEM (Fig. 2) prevents their realistic size estimation by DLS, the DLS data could be used for at-line monitoring of the nanotransformation process.

3.2.2. RSA of the DLS data and process modelling

With all measured DLS size and PDI data a response surface analysis (RSA) was carried out to relate the product variability to the process settings. The RSA allows to identify the important process parameters, quantify their relative importance and finally determine the "design space" within which the process should be operated, monitored and controlled [32].

From a statistical point of view, the size data at t = 0 differ significantly from the rest of the data. This means that the software considers often these data as outliers and these data will dominate the model if not excluded. Therefore, it is recommendable to use only the data from t = 20 min after starting the sonication. The multilinear regression analysis for all 66 sample data (for each of the 11 runs, the solution was measured every 20 min between t = 20 and t = 120), then allows to develop a robust model. A comparison of pre-treatments suggests to use a natural logarithmic transformation for the DLS size data. This linearizes the exponential particle size decay (first-order reaction, see Fig. 3A) during sonication and simplifies the model.

The final model has a R-squared of 0.85 and a relative error (coefficient of variation, CV) of around 2 %, which is reasonable bearing in mind the complex sample preparation procedure and the fact that the measurement of diluted particle dispersions may be affected by sedimentation of larger particles.

The model for the particle size (ln(DSL values)) includes all 4 factors as main effects (including reaction time) and additionally the AB interaction between US amplitude and flow rate. The regression coefficients of the ln(DLS) data are given in Table 3 in coded units (low = −1, high = +1) to ease interpretation.

The intercept is the mean of all particle sizes within this design which is around 900 nm (exp(6.81) = 906). All coefficients are negative except the AB interaction. The dominant factor is reaction time, as expected, followed by lignin concentration, which is 4 times smaller. The main effects flow rate and US amplitude are of minor importance but their interaction (AB) is the second important term in the regression model for particle size.

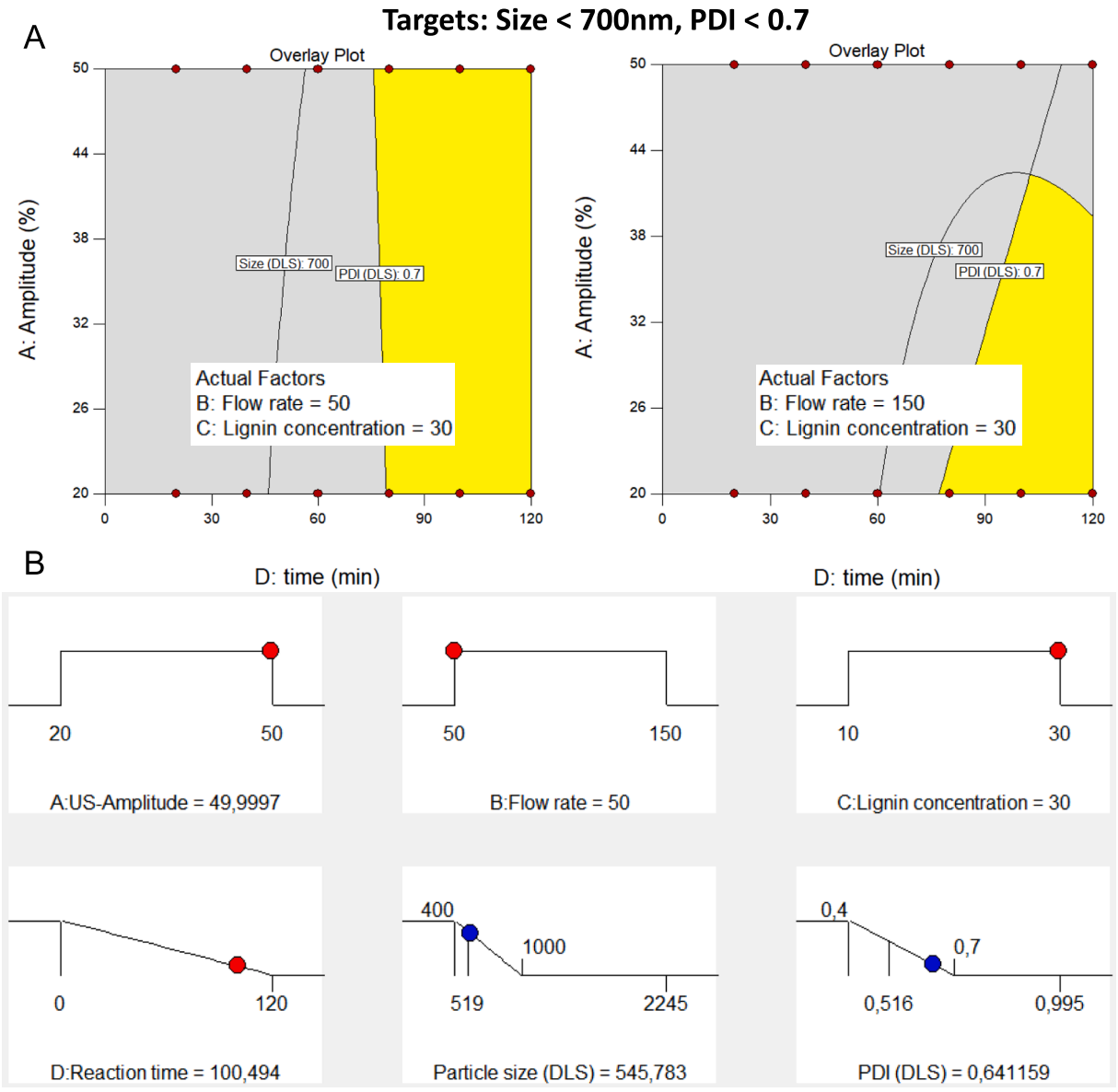

Fig. 6. Sonochemical process optimization to produce NPs with sizes < 700 nm and a PDI < 0.7. A) The yellow area shows the possible working area, where the targets are achieved. B) One possible solution out of the yellow working areas.

According to the model, the lowest size value is achieved with the following settings: reaction time high, lignin concentration high, flow rate low and US amplitude high. These settings result in a theoretical particle size of 450 nm (Fig. 4B). An almost identical particle size (470 nm) is achieved with high flow rate and low US amplitude and all the other factors high (Fig. 4D).

For practical applications it is also important to emphasize that due to the negative sign of factor C (lignin concentration), a higher concentration of lignin in the dispersion yields a higher percentage of smaller particles. This result was surprising, because high solution concentration usually promotes an increased collision frequency between the particles upon sonication, and often ends in more agglomeration. However, in this case, after 20 min, the lignin dispersion contains a mixture of NPs, larger particles and lignin in solution as described in 3.1.2. The collision among these colloidal species in more concentrated dispersions may result in further fractioning of the larger particles and size reduction. An increase of the initial lignin concentration that ensures high throughput would make the sonochemical process more attractive from a cost-performance perspective.

The same tendency for the particle polydispersity can be observed (Fig. 5), however, the models for PDI are generally less robust than for size. Unlike the nonlinearity of the statistical model for particle size, the polydispersity behaves almost linearly with respect to the duration of sonication and sample flow rate. The change of PDI could be neglected at low lignin concentrations, whereas at higher concentrations, the PDI decreases linearly reaching a minimum at low flow rates. Apparently, to optimize the energy impact of the sonication, a high number of particles are needed to collide, decreasing their size and polydispersity. At low lignin concentrations, the acoustic energy is rather dissipated in heating the water medium, with little effect on the size and polydispersity of the obtained NPs.

3.2.3. *Process optimization*

Using the established parameters, the model is able to simulate the experimental results to predict particle size and PDI, and can be used to design customized particle fractions. The targets for particle size are set to < 700 nm and PDI smaller 0.7 (Fig. 7A). For high lignin concentration the maximum possible working area is achieved for reaction times above 80 min, a low flow rate and it is independent of US amplitude. If the flow rate is set too high, the possible working area is decreased. The possible

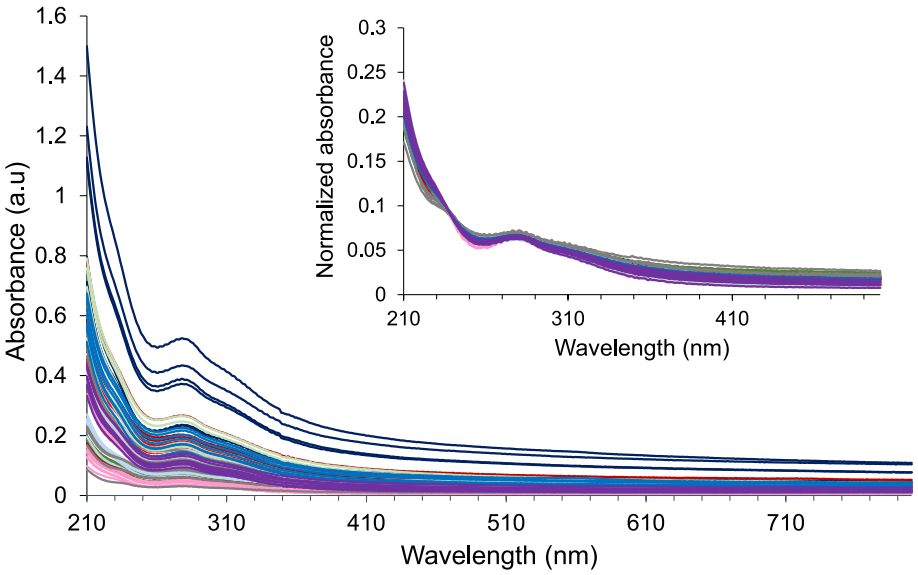

Fig. 7. Original spectra of all runs (taken every 20 min between t = 0 and t = 120 min) in the wavelength range 210 – 800 nm. Insert: Vector normalized spectra (Norm1) in the wavelength range between 210 nm and 500 nm.

working area is further reduced if higher US amplitudes are applied. However, it is worth mentioning that the major size reduction from several microns to around 1000 nm occurred during the first 20 min of sonication. Longer process duration yielded even smaller NPs and significant better homogeneity of the particles' distribution. For example, a possible solution to obtain NPs with size under 700 nm and PDI < 0.7 can be performed using the parameters setting of high concentration and US amplitude and low flow rate (Fig. 6B).

3.3. UV–Vis spectroscopic analysis during nano-transformation to potentially establish an in-line control

3.3.1. General approach and multivariate curve resolution (MCR)

Process analytical technology (PAT) has drawn an enormous interest in recent years. The reason for this is the need to further increase the productivity of manufacturing processes, but also the realization that knowledge-based production can provide customers with tailor-made products of certified quality. In parallel, the costs of complex measurement technologies have been dramatically reduced, and advances in information technology make it possible to process large volumes of data in real time. Spectroscopic methods, in particular, are able to generate data with high information content in just a few fractions of a second, objectively reflecting the actual product state at the molecular level [29].

In case of simple reaction mixtures, the spectral components can possibly be identified with real chemical constituents by comparing their spectral fingerprints with actual chemical absorbance patterns. In case of complex systems, such as dispersions of lignin particles with a broad particle size distribution, it is difficult to identify different components. Nevertheless, in the present study, we will show that optical spectroscopy in combination with MCR as part of Machine Learning (ML) toolboxes can be used to analyze complex processes and materials [33]. The great advantage of the method is that information about the spectra of the "pure components" is not necessary, because those "pure" spectra are calculated directly from the mixtures. Furthermore, it is possible to get spectral information of the intermediate products, together with concentrations of all components over the reaction time.

3.3.2. UV–Vis spectroscopy to evaluate the spectral signature of the lignin particles. Spectral features and MCR

3.3.2.1. Spectral features. Molecular spectroscopy is based on the interaction of electromagnetic radiation with particulate matter. The inelastic interaction (photon impact on a molecule) results in the transition of the molecule from a lower to a higher energy level (absorption spectroscopy), whereas the elastic interaction with particulate matter results in the scatter of the photon in different directions (ELS = elastic light spectroscopy, or Mie-backscatter spectroscopy) [29]. Both, elastic and inelastic interactions are wavelength dependent, and thus provide mostly superposed absorption and scatter spectra (labelled also as backscattering spectra).

UV peaks of lignin absorbance can be identified around 230 nm, 280 and 330 nm (Fig. 7). The different slopes of the spectra indicate the change of particle size during sonication due to Mie-scatter. For MCR calculation, the vector normalization (norm1) is used to compensate parallel shifts of the absorbance due to, e.g., sedimentation of particles during measurement.

3.3.2.2. MCR: component spectra. Interestingly, the mathematical deconvolution of the full spectral features (process trajectories) of the sonication reaction yields only three independent components, despite the complexity of the studied system. Using three components, the total residual (which represent the part of the data set that is not explained by the calculated model) is low (about 10^{-5} absorbance units). The use of a larger number of spectral components does not lead to any significant improvement in accuracy. This indicates that the chemistry of lignin is essentially determined by the mutual conversion of three spectroscopically distinguishable chemical functionalities. Further constraints used in the MCR calculations are non-negativity for the calculated component spectra and corresponding concentrations arrays. As the aim of this investigation was the study of lignin transformation kinetics, the constraint closure was also applied to the calculated concentrations. This means that all calculated concentrations are added to 1, which is then equivalent to 100 %. This highlights the changes in the spectra and it allows in this case the study of the kinetics in the formation (change of concentration vs. time) of the nanoparticles regardless of the initial concentration of lignin particles.

The "pure spectrum" of component 2 (red) can clearly be associated with the important lignin peaks at 230 and 280 nm (Fig. 8A). This MCR-

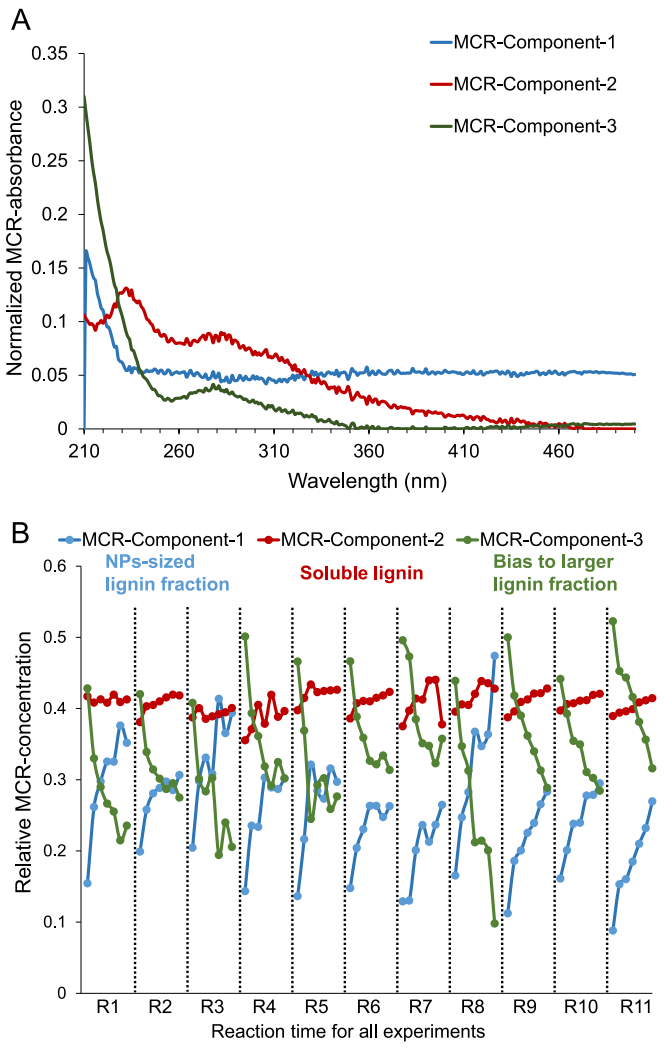

Fig. 8. A) MCR calculated "pure spectra" (fundamental spectral features) of LigNPs reaction spectra. Spectra are vector normalized (Norm1 for wavelength range 210 – 500 nm.). B) Concentration profiles of the 3 calculated MCR component spectra during sonication for t = 0–120 min reaction time for all 11 experiments. Concentrations are given in relative MCR concentration units.

Table 4
Coefficients of model terms of the response surface analysis for response MCR component 3 (large particle fraction).

Intercept: +32,9	A-US amplitude + 0.31
B-Flow rate:+0.36	C-Lignin concentration:+0.95
D-time: −8.47	AB-interaction:-2.92
BC-interaction:+1.26	

component was labelled as "soluble lignin". The spectrum of component 1 (blue) shows a constant high absorbance starting from wavelength 340 nm. Mie-scatter simulations using the software "Mie-Plot" (Philip Laven) confirm these spectral features [34]. Consequently, this spectrum of component 1 can be assigned to the smaller NPs. The spectrum for component 3 (green) has high absorbance in the UV region below 240 nm and shows no distinct peaks.

3.3.2.3. MCR: Evolution of the pure component concentrations during sonication. For each of the 11 experiments, the concentrations of the three components were calculated during the sonication process (from t = 0 to t = 120 min). (Fig. 8B). The soluble lignin (component 2, red) accounts for a nearly constant amount of 40 % of the total spectral reaction mixture for all reactions. Component 3 (green) decreases during sonication whereas component 1 (blue) increases. This suggests that component 3 can be assigned to the larger lignin particles and component 1 to the nanoparticles. The given concentration profiles are "spectroscopic concentrations" and may be different to the weighted concentrations. The spectral concentrations are biased by the extinction, respectively the scatter coefficients of the particles.

How much the concentration of component 1 and 3 change over time depends on the settings of the reaction parameters. The obtained results clearly demonstrate that in-line process design and control is a feasible option for the future.

3.3.3. Process optimization on a molecular level using the component spectra and component concentrations

The calculated MCR component concentrations can be regarded as measured concentrations, and one can use them to calculate a process model for the reaction settings used. As the concentration of component 2 (soluble lignin) remains nearly constant for all experiments, a process model is not feasible. Component 3 and 1 are complementary as the decrease of component 3 results in an increase of component 1. Table 4 gives as an example for a process model the estimated coefficients for the larger particles (component 3). The model is given in coded units to ease interpretation.

The RSA leads to a similar model as the DLS data, with an intercept value of 32.9 % (Table 4). This is the mean value of all measured component 3 values and represents the model center. The parameter D: time has the major influence on the decrease of component 3. Factor A: US amplitude, B: flow rate and C: lignin concentration are not significant as main effects, but they are involved in interactions and therefore also influence the behavior of component 3. The second important term is the AB-interaction between US amplitude and flow rate. In the DLS model higher lignin concentration decreased particle size. Here it is the BC-interaction (flow rate and lignin concentration) that is responsible for the decrease of particle size. This can be explained by the transformation of absolute intensities due to vector normalization of the spectra. In addition, the spectral intensities of the 3 MCR components were normalized to 1 (100 %). Thus, only relative changes can be considered. The behavior of component 3 as a function of time and flow rate is shown in Fig. 9 for low (Fig. 9A) and high amplitude (Fig. 9B) settings.

Major chances in component 3 occur within the first 60 min. Prolonged sonication from 60 to 120 min results only in minor changes especially for low flow rates (Fig. 9A). For higher flow rates, smaller particles were obtained in shorter time (Fig. 9B). As discussed also in the DLS data section, it seems that 60 min of sonication together with high lignin concentration and high flow rate may be a favorable process setting for production of NPs with high throughput.

4. Conclusions

In this work, we present a large-scale continuous ultrasound assisted waterborne lignin nanotrasnformation process with high reaction yield. The process was designed and monitored using methods of statistical DoE and analyzing the optical spectroscopic features (DLS and UV–Vis) of lignin during sonication. Here, we used a two-level factorial design with three variables – raw material concentration, flow rate and amplitude - to understand the sonochemical process of lignin nanotransformation. The data resulted from DoE was studied by RSA and MCR allowing to determine both qualitatively and quantitatively the "cause and effect". The initial 20 min of sonication notably reduced the particle size from more than 2500 nm to roughly 1000 nm and even less. Afterwards, the lignin fragmentation into nanoparticles followed a moderate particle size decrease to below 700 nm until the end of the 2 h process. The RSA model of DLS measurement revealed that lignin concentration and sonication time were the most important factors to achieve smaller size NPs. Surprisingly, higher raw material concentration

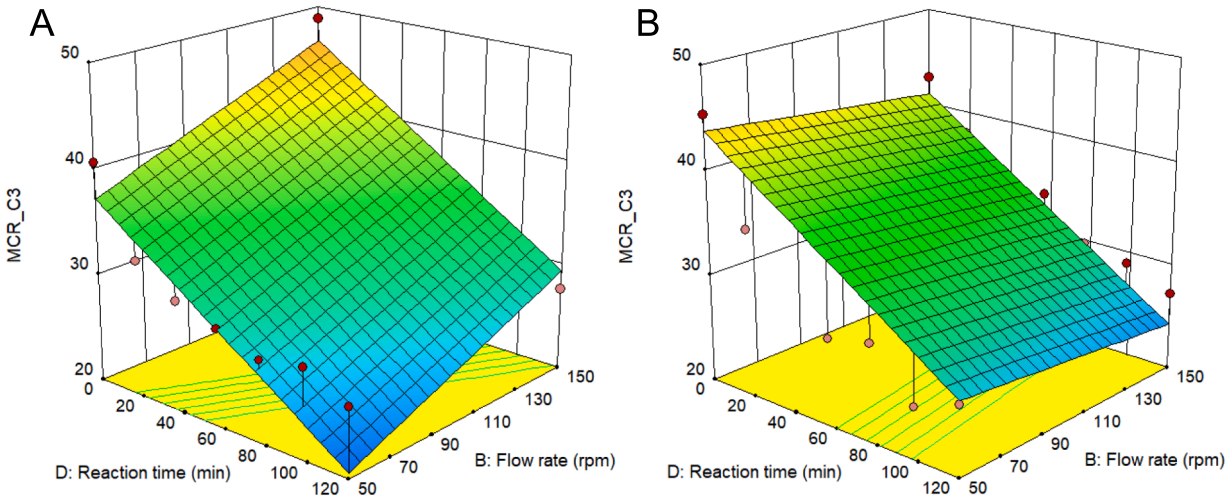

Fig. 9. Response surface-plots of MCR component 3 (spectral response of the fraction of larger particle sizes) over time and flow rate at high lignin concentrations and A) low and B) high US amplitude settings.

resulted in the synthesis of smaller nanoparticles, probably due to an increase in the number of particles' collision, leading to fragmentation of the biomass. A strong relationship between flow rate and sonication amplitude was also disclosed. The lowest size values were obtained with high amplitudes and low flow rates, and *vice versa*.

The model was qualified with a Rsquared of 0.89 and a CV of about 2 %, which can be considered reasonable given the heterogeneity of the original material and the multi-step sampling process. Due to the robustness of the model, it may be used to predict the size and polydispersity of the sonicated lignin with different parameter settings and thus create customized particle fractions. In the case of the UV–Vis spectroscopy, the spectral features of the different lignin fractions could be attributed and estimated using the component spectra of the MCR calculation. The results were consistent with the DLS measurements and RSA model. These findings would enable the application of UVVis spectroscopy for in-line monitoring and comprehensive management of an industrial process for lignin nanotransformation.

5. Author's contribution

S.P-R.: Experimental design, lignin nanoparticles preparation and characterization in continuous mode, results analysis, figures design, manuscript writing, project administration; G.F. Lignin nanoparticles characterization in continuous mode, results analysis, figures design, manuscript writing; R.K. interpretation of the spectroscopic results, manuscript writing; W.K.: DoE response analysis and MCR calculations, manuscript writing; J. B.: Lignin sonicated dispersion characterization, figures design; G.R.; Lignin sonicated dispersion characterization, manuscript revision; A.G.M: Synthesis and characterization of lignin nanoparticles at lab-scale, figures design, manuscript revision; T.T.: experiments design, manuscript writing and revision, project administration, funding acquisition.

Funding

This research was funded by the European Union under the framework of the projects BIOMAT (H2020-953270) and rLightBioCom (HORIZON-101091691). G. F. acknowledges Universitat Politècnica de Catalunya and Banco Santander for his PhD grant (113 FPI-UPC 2018).

CRediT authorship contribution statement

Sílvia Pérez-Rafael: Project administration, Conceptualization, Investigation, Validation, Writing – original draft, Writing – review & editing. **Tzanko Tzanov:** Project administration, Funding acquisition, Conceptualization, Supervision, Writing – original draft, Writing – review & editing.

Declaration of Competing Interest

The authors declare that they have no known competing financial interests or personal relationships that could have appeared to influence the work reported in this paper.

References

[1] A.J. Ragauskas, G.T. Beckham, M.J. Biddy, R. Chandra, F. Chen, M.F. Davis, B. H. Davison, R.A. Dixon, P. Gilna, M. Keller, P. Langan, A.K. Naskar, J.N. Saddler, T. J. Tschaplinski, G.A. Tuskan, C.E. Wyman, Lignin valorization: improving lignin processing in the biorefinery, Science 344 (2014) 1246843, https://doi.org/10.1126/science.1246843.
[2] H. Sixta, Raw material for pulp, in: Handbook of Pulp, WILEY-VCH, Germany, 2006, https://doi.org/10.1002/9783527619887ch1.
[3] N.E. El Mansouri, J. Salvadó, Structural characterization of technical lignins for the production of adhesives: application to lignosulfonate, kraft, soda-anthraquinone, organosolv and ethanol process lignins, Ind. Crops Prod. 24 (2006) 8–16, https://doi.org/10.1016/j.indcrop.2005.10.002.
[4] J.A. Poveda-Giraldo, J.C. Solarte-Toro, C.A. Cardona Alzate, The potential use of lignin as a platform product in biorefineries: A review, Renew. Sustain. Energy Rev. 138 (2021) 110688, https://doi.org/10.1016/j.rser.2020.110688.
[5] B.M. Upton, A.M. Kasko, Strategies for the conversion of lignin to high-value polymeric materials: Review and perspective, Chem. Rev. 116 (2016) 2275–2306, https://doi.org/10.1021/acs.chemrev.5b00345.
[6] V.K. Thakur, M.K. Thakur, P. Raghavan, M.R. Kessler, Progress in green polymer composites from lignin for multifunctional applications: A review, ACS Sustain. Chem. Eng. 2 (2014) 1072–1092, https://doi.org/10.1021/sc500087z.
[7] R. de Avila Delucis, W.L.E. Magalhães, C.L. Petzhold, S.C. Amico, Forest-based resources as fillers in biobased polyurethane foams, J. Appl. Polym. Sci. 135 (2018) 1–7, https://doi.org/10.1002/app.45684.
[8] M. Oliviero, L. Verdolotti, E. Di Maio, M. Aurilia, S. Iannace, Effect of supramolecular structures on thermoplastic zein-lignin bionanocomposites, J. Agric. Food Chem. 59 (2011) 10062–10070, https://doi.org/10.1021/jf201728p.
[9] M. Lee, H.S. Jeon, S.H. Kim, J.H. Chung, D. Roppolo, H.-J. Lee, H.J. Cho, Y. Tobimatsu, J. Ralph, O.K. Park, Lignin-based barrier restricts pathogens to the infection site and confers resistance in plants, EMBO J 38 (2019), e101948, https://doi.org/10.15252/embj.2019101948.
[10] G. Wang, Y. Xia, B. Liang, W. Sui, C. Si, Successive ethanol–water fractionation of enzymatic hydrolysis lignin to concentrate its antimicrobial activity, J. Chem. Technol. Biotechnol. 93 (2018) 2977–2987, https://doi.org/10.1002/jctb.5656.
[11] A. Zeb, Concept, mechanism, and applications of phenolic antioxidants in foods, J. Food Biochem. 44 (2020) e13394, doi: 10.1111/jfbc.13394.
[12] B. Wang, D. Sun, H.M. Wang, T.Q. Yuan, R.C. Sun, Green and facile preparation of regular lignin nanoparticles with high yield and their natural broad-spectrum sunscreens, ACS Sustain. Chem. Eng. 7 (2019) 2658–2666, https://doi.org/10.1021/acssuschemeng.8b05735.
[13] Y. Qian, X. Zhong, Y. Li, X. Qiu, Fabrication of uniform lignin colloidal spheres for developing natural broad-spectrum sunscreens with high sun protection factor,

Ind. Crops Prod. 101 (2017) 54–60, https://doi.org/10.1016/j.indcrop.2017.03.001.
[14] A. Grossman, V. Wilfred, Lignin-based polymers and nanomaterials, Curr. Opin. Biotechnol. 56 (2019) 112–120, https://doi.org/10.1016/j.copbio.2018.10.009.
[15] Z. Zhang, V. Terrasson, E. Guénin, Lignin nanoparticles and their nanocomposites, Nanomaterials 11 (2021) 1336, https://doi.org/10.3390/nano11051336.
[16] B. Del Saz-Orozco, M. Oliet, M.V. Alonso, E. Rojo, F. Rodríguez, Formulation optimization of unreinforced and lignin nanoparticle-reinforced phenolic foams using an analysis of variance approach, Compos. Sci. Technol. 72 (2012) 667–674, https://doi.org/10.1016/j.compscitech.2012.01.013.
[17] E. Cavallo, X. He, F. Luzi, F. Dominici, P. Cerrutti, C. Bernal, M.L. Foresti, L. Torre, D. Puglia, U.V. Protective, Antioxidant, antibacterial and compostable polylactic acid composites containing pristine and chemically modified lignin nanoparticles, Molecules 26 (2020) 126, https://doi.org/10.3390/molecules26010126.
[18] A.G. Morena, Pérez-Rafael-Sílvia, T. Tzanov, Lignin-Based Nanoparticles as Both Structural and Active Elements in Self-Assembling and Self-Healing Multifunctional Hydrogels for Chronic Wound Management, Pharmaceutics. 14 (2022) 2658, doi:10.3390/pharmaceutics14122658.
[19] S. Pérez-Rafael, K. Ivanova, I. Stefanov, J. Puiggalí, L.J. del Valle, K. Todorova, P. Dimitrov, D. Hinojosa-Caballero, T. Tzanov, Nanoparticle-driven self-assembling injectable hydrogels provide a multi-factorial approach for chronic wound treatment, Acta Biomater. 134 (2021) 131–143, https://doi.org/10.1016/j.actbio.2021.07.020.
[20] P.K. Mishra, R. Wimmer, Aerosol assisted self-assembly as a route to synthesize solid and hollow spherical lignin colloids and its utilization in layer by layer deposition, Ultrason. Sonochem. 35 (2017) 45–50, https://doi.org/10.1016/j.ultsonch.2016.09.001.
[21] D. Piccinino, E. Capecchi, E. Tomaino, S. Gabellone, V. Gigli, D. Avitabile, R. Saladino, Nano-structured lignin as green antioxidant and uv shielding ingredient for sunscreen applications, Antioxidants. 10 (2021) 274, https://doi.org/10.3390/antiox10020274.
[22] M. Tortora, F. Cavalieri, P. Mosesso, F. Ciaffardini, F. Melone, C. Crestini, Ultrasound driven assembly of lignin into microcapsules for storage and delivery of hydrophobic molecules, Biomacromolecules 15 (2014) 1634–1643, https://doi.org/10.1021/bm500015j.
[23] S. Iravani, R.S. Varma, Greener synthesis of lignin nanoparticles and their applications, Green Chem. 22 (2020) 612–636, https://doi.org/10.1039/c9gc02835h.
[24] C. Frangville, M. Rutkevičius, A.P. Richter, O.D. Velev, S.D. Stoyanov, V. N. Paunov, Fabrication of environmentally biodegradable lignin nanoparticles, ChemPhysChem 13 (2012) 4235–4243, https://doi.org/10.1002/cphc.201200537.
[25] F. Gomollón-Bel, IUPAC Top Ten Emerging Technologies in Chemistry 2021, Chem. Int. 43 (2021) 13-20, doi: 10.1515/ci-2021-0404.
[26] I.A. Gilca, V.I. Popa, C. Crestini, Obtaining lignin nanoparticles by sonication, Ultrason. Sonochem. 23 (2015) 369–375, https://doi.org/10.1016/j.ultsonch.2014.08.021.
[27] M.N. Garcia Gonzalez, M. Levi, S. Turri, G. Griffini, Lignin nanoparticles by ultrasonication and their incorporation in waterborne polymer nanocomposites, J. Appl. Polym. Sci. 134 (2017) 45318, https://doi.org/10.1002/app.45318.
[28] A.K. Naskar, J.K. Keum, R.G. Boeman, Polymer matrix nanocomposites for automotive structural components, Nat. Nanotechnol. 11 (2016) 1026–1030, https://doi.org/10.1038/nnano.2016.262.
[29] R.W. Kessler, M. Maiwald, W. Kessler, Inline and online process analytical technology with a focus on optical spectroscopy, Encycl. Anal. Chem. (2022) 1–31, https://doi.org/10.1002/9780470027318.a9791.
[30] A.G. Morena, A. Bassegoda, M. Natan, G. Jacobi, E. Banin, T. Tzanov, Antibacterial properties and mechanisms of action of sonoenzymatically synthesized lignin-based nanoparticles, ACS Appl. Mater. Interfaces. 14 (2022) 37270–37279, https://doi.org/10.1021/acsami.2c05443.
[31] H.K.S. Souza, J.M. Campiña, A.M.M. Sousa, F. Silva, M.P. Gonçalves, Ultrasound-assisted preparation of size-controlled chitosan nanoparticles: characterization and fabrication of transparent biofilms, Food Hydrocoll. 31 (2013) 227–236, https://doi.org/10.1016/j.foodhyd.2012.10.005.
[32] G.E.P. Box, J.S. Hunter, W.G. Hunter. Statistics for Experimenters: Design, Innovation and Discovery, second ed.,Wiley, 2005. New York.
[33] J. Jaumot, A. de Juan, R. Tauler, MCR-ALS GUI 2.0: New features and applications, Chemom. Intell. Lab. Syst. 140 (2015) 1–12, https://doi.org/10.1016/j.chemolab.2014.10.003.
[34] MiePlot, (n.d.). www.philiplaven.com/mieplot.htm.